

# Chalcophile elements in post-subduction magmas and implications for long-term metal recycling in oceanic and continental subduction

Xiang Wang<sup>a</sup>, Zaicong Wang<sup>a, 1, \*</sup>, Li-Qun Dai<sup>b, 1</sup>, Wen Zhang<sup>a</sup>, Xiaodong Deng<sup>c</sup>, Xi Zhang<sup>d</sup>, Stephen Foley<sup>e</sup>, Charles H. Langmuir<sup>f</sup>, Wei Fang<sup>b</sup>, Lang Wang<sup>a</sup>, Tao He<sup>a</sup>, Aiqing Ren<sup>a</sup>, Zhaochu Hu<sup>a</sup>, Keqing Zong<sup>a</sup>, Yongsheng Liu<sup>a</sup>, Jianwei Li<sup>c</sup>, Huai Cheng<sup>g</sup>, Pingyang Zhang<sup>h</sup>

<sup>a</sup>State Key Laboratory of Geological Processes and Mineral Resources, School of Earth Sciences, China University of Geosciences, Wuhan 430074, China

<sup>b</sup>Chinese Academy of Sciences (CAS) Key Laboratory of Crust-Mantle Materials and Environments, School of Earth and Space Sciences, University of Science and Technology of China, Hefei 230026, China

<sup>c</sup>State Key Laboratory of Geological Processes and Mineral Resources, School of Earth Resources, China University of Geosciences, Wuhan 430074, China

<sup>d</sup>China Minmetals Exploration and Development CO., LTD, Beijing, China

<sup>e</sup>School of Natural Sciences, Macquarie University, Sydney, New South Wales 2109, Australia

<sup>f</sup>Department of Earth and Planetary Sciences, Harvard University, Cambridge, MA 02138, USA

<sup>g</sup>Guangzhou Marine Geological Survey, China Geological Survey, Guangzhou 510075, China

<sup>h</sup>Yantai Center of Coastal Zone Geological Survey, China Geological Survey, Yantai 264000, China

\*Correspondence to Zaicong Wang (zaicongwang@cug.edu.cn).

<sup>1</sup>These authors contributed equally to this work.

## Electronic Annex A: Supplementary figures

Fig. S1

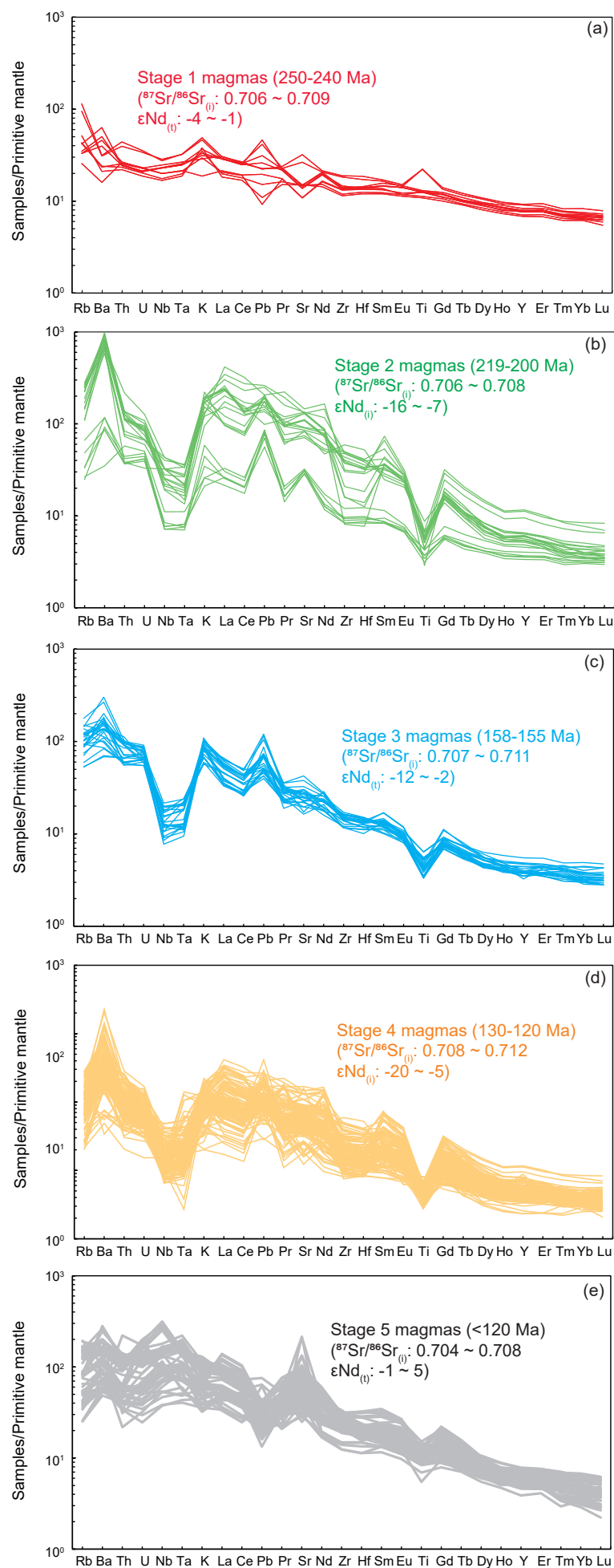


Fig. S1: Primitive mantle-normalized trace element patterns for Mesozoic mafic magmas in the eastern NCC. Stage 1 and 5 magmas display OIB-like trace element patterns with slightly elevated Ba/Nb ratios (10 - 20). In contrast, stage 2, 3, and 4 magmas display arc-like trace element patterns with much higher Ba/Nb ratios (100 - 500). Data sources: trace element contents and radiogenic Sr-Nd isotopes of Mesozoic mafic magmas in the NCC (Fang et al., 2020a; Fang et al., 2019; Fang et al., 2020b; Jiang et al., 2010; Wang et al., 2020a; Xu et al., 2016; Zhao et al., 2012 and references therein).

Fig. S2

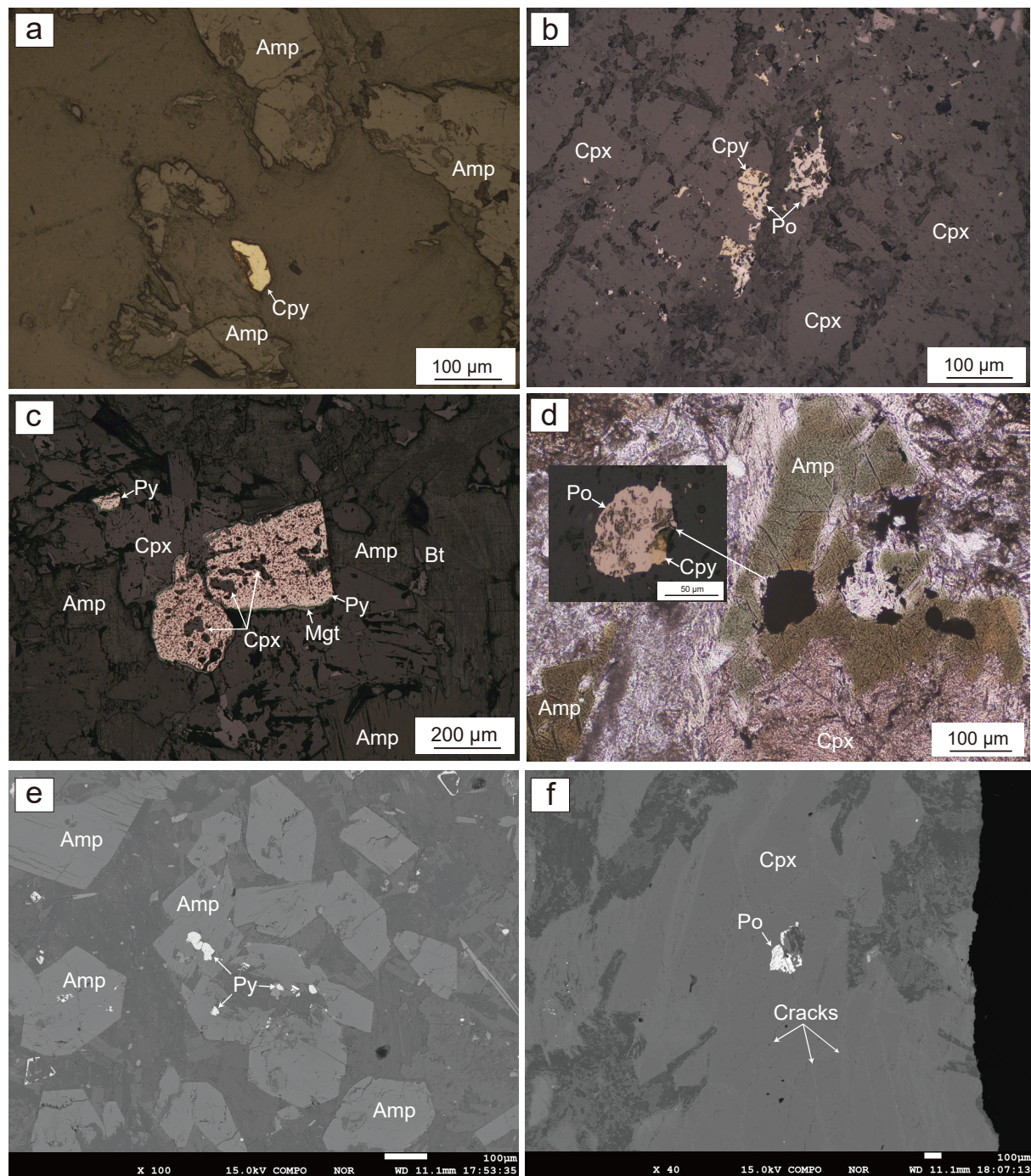


Fig. S2: Photomicrographs of sulfides in the Early Triassic to Late Jurassic mafic rocks in the eastern NCC. (a, b, c) The sulfides in these rocks are chalcopyrite, pyrrhotite, and pyrite, and most of them formed interstitially to phenocrysts such as clinopyroxene and amphibole. Several silicate minerals can be observed as inclusion in large grains of pyrite. This indicates that most sulfides crystallized at the late stage of magmatic evolution. (d, e, f) Very few sulfide inclusions can be observed in amphibole and clinopyroxene phenocrysts. Amp - amphibole, Cpx - clinopyroxene, Bt - biotite, Cpy - chalcopyrite, Po - pyrrhotite, Py - pyrite, Mgt - magnetite.

Fig. S3

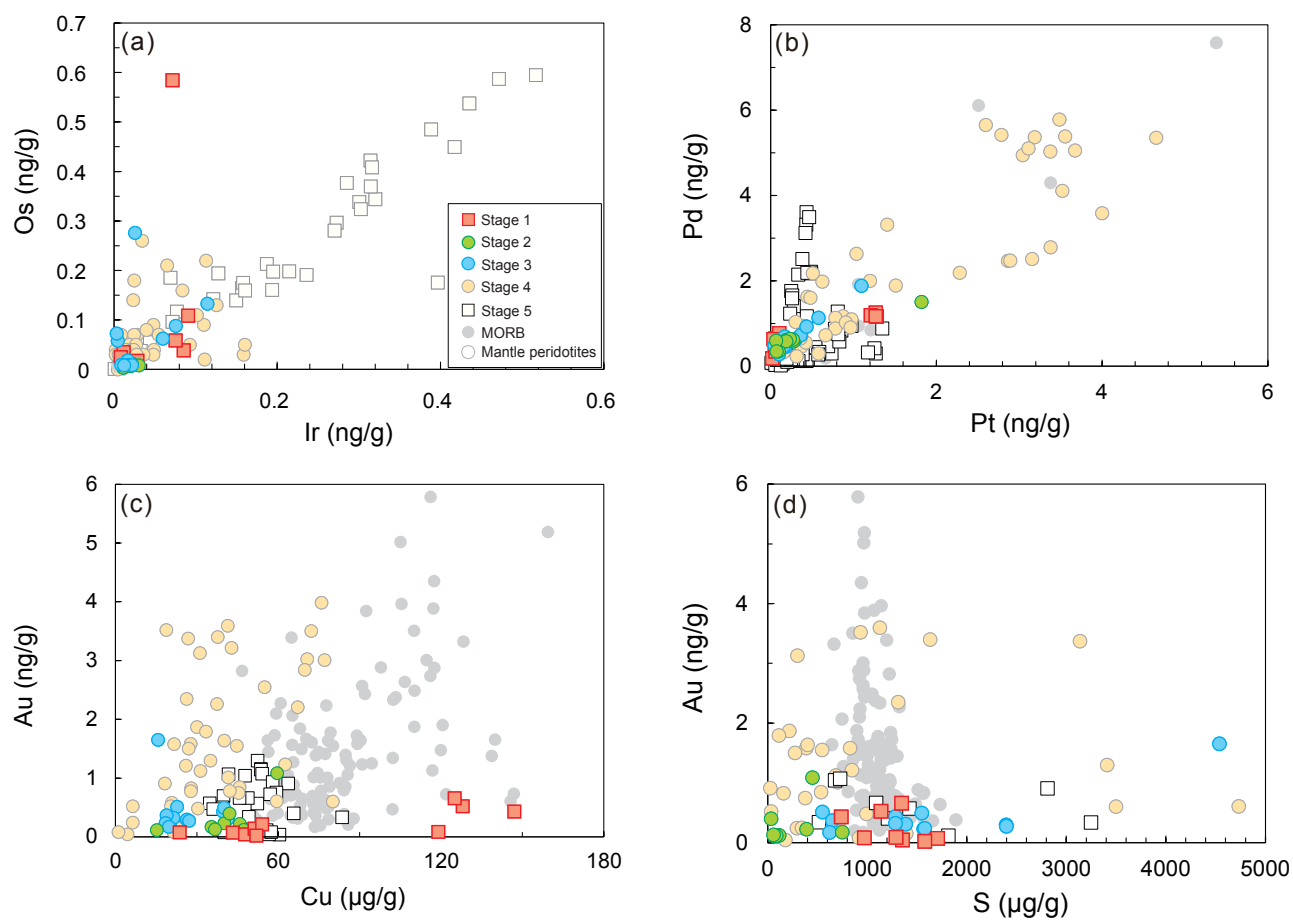


Fig. S3: PGE, Au, Cu, and S contents of Mesozoic magmas in the eastern NCC. The PGE in Mesozoic magmas correlates positively with each other. Their Au shows broadly positive correlation with Cu and S, and those samples with high Au but low S contents may reflect the Au enrichment in the mantle source (Wang et al., 2022). Data source is the same as Fig. 2.

Fig. S4

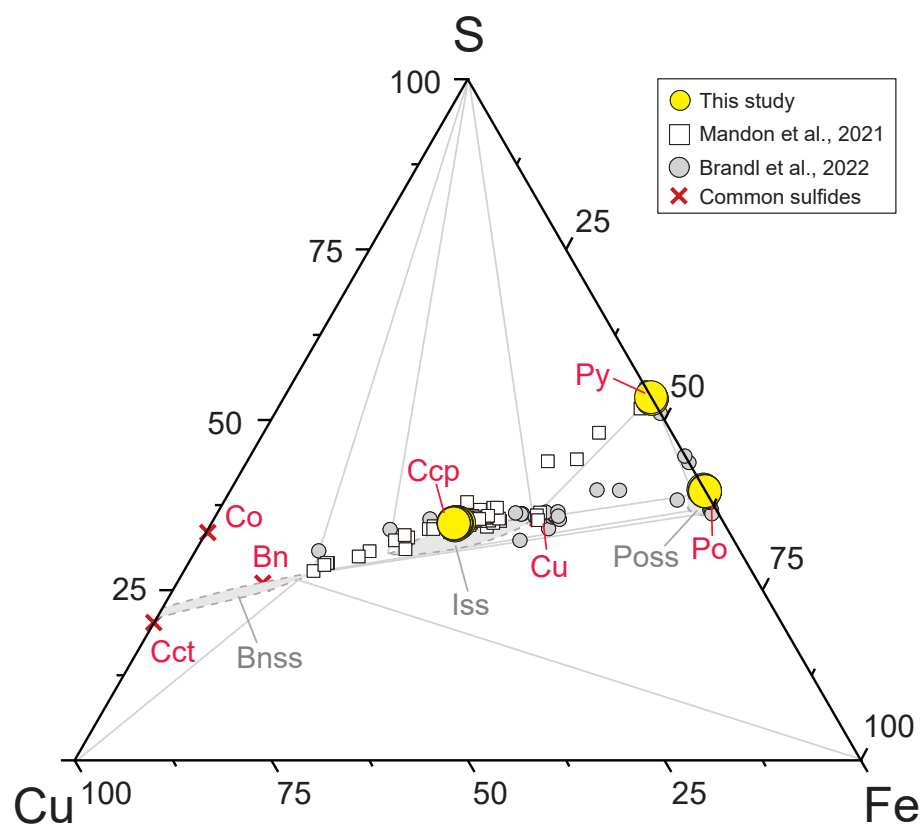


Fig. S4: The major composition of sulfides. Sulfides in mafic rocks from the eastern NCC are chalcopyrites, pyrrhotites, and pyrites. Combined with their distribution and shapes, this indicates the magmatic origins of these sulfides. The sulfide phase diagram at 1100 °C is modified from Kullerud et al. (1969), and typical magmatic sulfides are presented for comparison (Brandl et al., 2022; Mandon et al., 2021).



Fig. S5

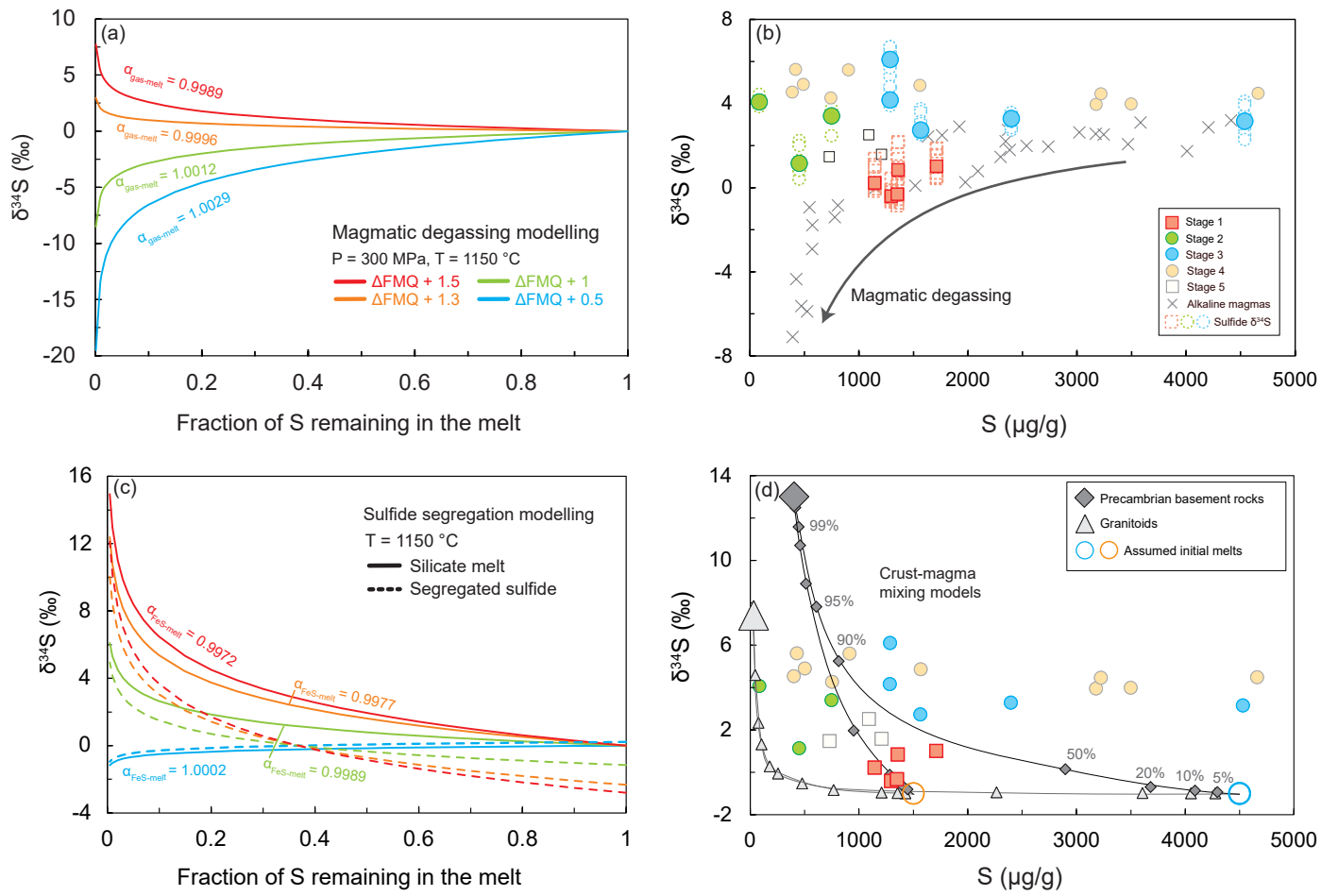


Fig. S5: Effects of magmatic and surface processes on  $\delta^{34}\text{S}$  variation of Mesozoic magmas in the NCC. (a) Modelling of S isotope fractionation during magmatic degassing. The total S isotope value ( $\delta^{34}\text{S}\Sigma\text{S}$ ) of primary melts is assumed to be at 0 ‰ and oxygen fugacity ( $f\text{O}_2$ ) of  $\Delta\text{FMQ} + 0.5$ ,  $+1$ ,  $+1.3$  and  $+1.5$  are set for calculation in open-system processes, with a temperature of 1150 °C and pressure of 300 MPa, following the empirical equations provided by Marini et al. (2011) and Beaudry et al. (2018). The gas-melt equilibrium S isotope fractionation factor  $\alpha_{\text{gas-melt}}$  is calculated as 1.0029, 1.0012, 0.9996, and 0.9989 for  $f\text{O}_2$  ranging from  $\Delta\text{FMQ} + 0.5$  to  $+1.5$ , respectively, using the empirical model of Marini et al. (2011) and fractionation factors from Fiege et al. (2015). The divergence in paths is primarily determined by  $f\text{O}_2$ , transitioning from a system dominated by  $\text{S}^{2-}$  ( $\text{H}_2\text{S}$ ) where  $\alpha_{\text{gas-melt}} > 1$ , to one dominated by  $\text{S}^{6+}$  ( $\text{SO}_4^{2-}$ ) where  $\alpha_{\text{gas-melt}} < 1$  (Jugo et al., 2010). (b) Whole-rock S contents and sulfide  $\delta^{34}\text{S}$  in Mesozoic magmas. The  $\delta^{34}\text{S}$  values of these magmas are calculated from the mean  $\delta^{34}\text{S}$  values of sulfide (filled circles and rectangles). Despite the large range of S contents in Mesozoic magmas, the sulfide  $\delta^{34}\text{S}$  in each episode of magmas shows narrow ranges, regardless of sulfide type and sulfide distribution. Data source: degassed alkaline magmas (Beaudry et al., 2018), stage 4 and 5 magmas (Wang et al., 2024). (c) Modelling of S isotope fractionation between silicate melts and segregated sulfides. The equations are from Marini et al. (2011) and the same parameters of temperatures,  $f\text{O}_2$ , and S speciation in melts as detailed above are used. The computed fractionation factors  $\alpha_{\text{FeS-melts}}$  range from 0.9972 to 1.0002. Under slightly oxidized conditions ( $f\text{O}_2$  of  $\Delta\text{FMQ} + 0.5$ ), the S isotope fractionation between segregated sulfides and silicate melts is limited (0.2 ‰). However, under highly oxidized conditions ( $f\text{O}_2 > \Delta\text{FMQ} + 1$ ), the segregated sulfides have lower  $\delta^{34}\text{S}$  values than silicate melts, with S isotope fractionation increasing with  $f\text{O}_2$ , from 1.1 ‰ ( $\Delta\text{FMQ} + 1$ ) to 2.8 ‰ ( $\Delta\text{FMQ} + 1.5$ ). As a result, the  $\delta^{34}\text{S}$  of remaining melts increases with sulfide segregation. (d) Binary mixing model of crustal contamination during melt ascent. The lines show end-member mixing between primitive mantle melts (with  $\delta^{34}\text{S} = -1$  ‰ and S contents of 1000 and 4500 μg/g) and granitoids (with average  $\delta^{34}\text{S} = 7.4$  ‰ and S contents of 30 μg/g), Precambrian basement rocks (with average  $\delta^{34}\text{S} = 13$  ‰ and S contents of 402 μg/g) (Deng et al., 2020; Wang et al., 2021; Xu et al., 2022; Zhao et al., 2022). The high S isotopes of these samples cannot be acquired by mixing between assumed initial mantle-derived magmas and regional granitoids, and it requires very high degrees of crustal contamination by basement rocks (20% - 90%) to account for their high  $\delta^{34}\text{S}$  values. These ratios are unlikely and cannot explain the high S, MgO, Cr, and Ni contents of most samples.

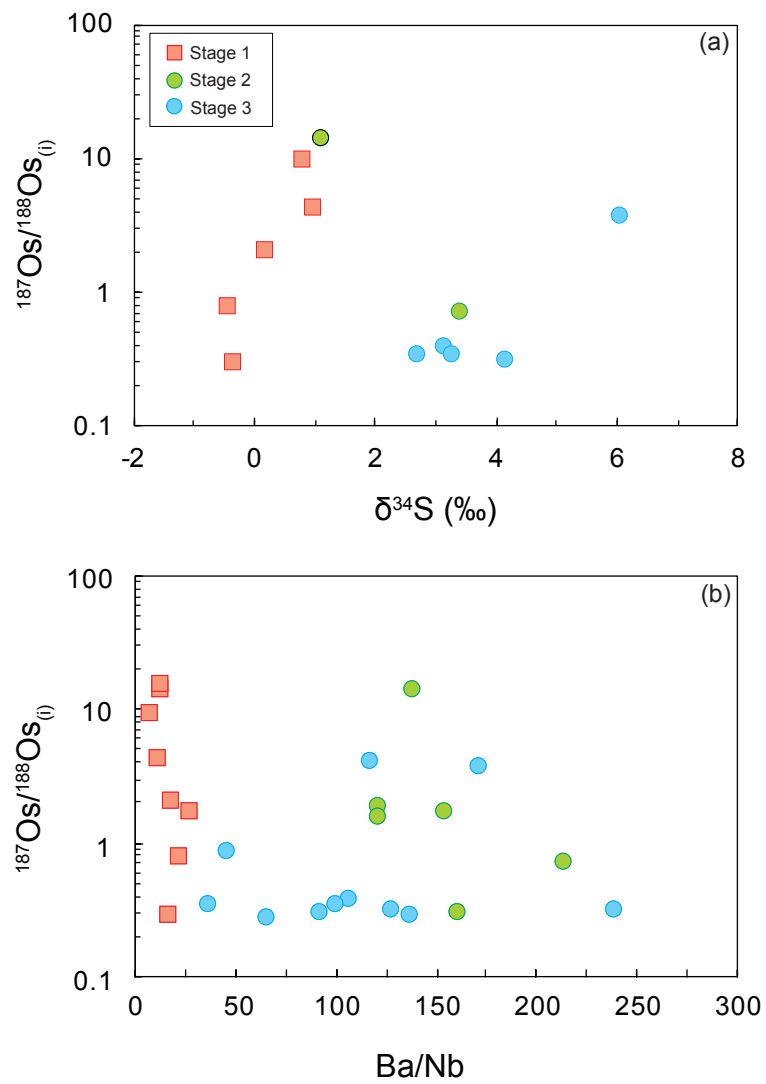


Fig. S6:  $^{187}\text{Os}/^{188}\text{Os}$ ,  $\delta^{34}\text{S}$ , and Ba/Nb ratios of stage 1-3 magmas. Samples with low Os,  $\delta^{34}\text{S}$ , and Ba/Nb values display high  $^{187}\text{Os}/^{188}\text{Os}$  values, indicating their radiogenic Os were unrelated to subduction addition. These extremely high  $^{187}\text{Os}/^{188}\text{Os}$  values may not be indicative of mantle source but reflect the crustal contamination or Re-Os disequilibrium.

Fig. S7

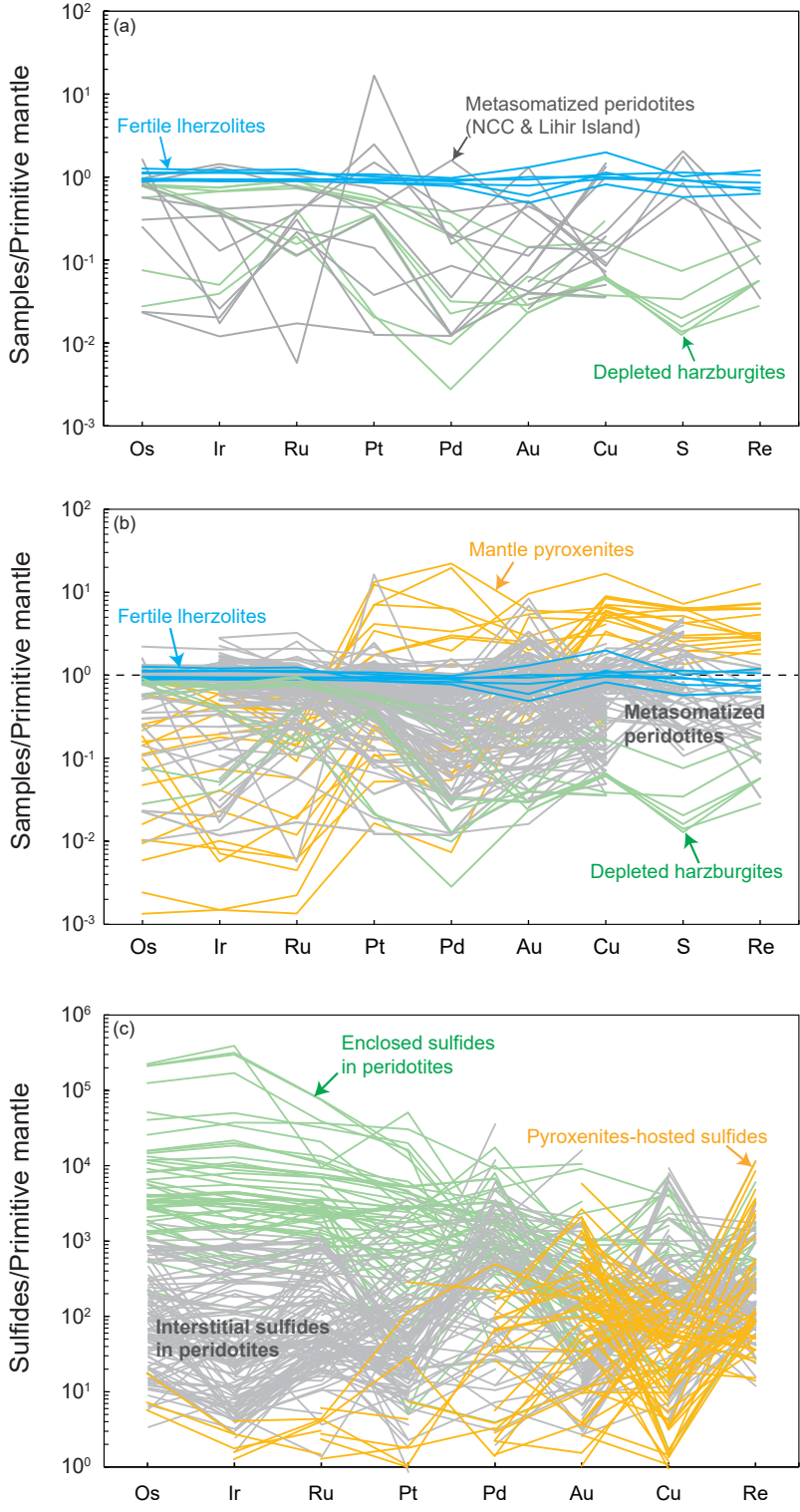


Fig. S7: Primitive mantle normalized PGE, Au, Cu, S, and Re contents for global mantle peridotites, pyroxenites, and sulfides. (a) The fertile lherzolites generally show chalcophile metal patterns akin to the primitive mantle. After high degrees of mantle melting, mantle residues are highly depleted in Pt, Pd, Au, Cu, S, and Re (e.g., harzburgites). However, even after strong metasomatism related to subduction, the mantle peridotites in the NCC and Lihir island still display relatively low contents of chalcophile metals (mostly lower than fertile peridotites). (b) The mantle metasomatism by pyroxenite melts or oxidized fluids may replenish chalcophile metals into the depleted mantle, and global metasomatized peridotites thus exhibit transitional chalcophile metal patterns between depleted harzburgites and fertile lherzolites. Some orogenic peridotites with native Au nanoparticles could have high Au contents ( $> 10$  ng/g), suggesting heterogeneous precipitation from volatile-rich melts, yet most samples do not show such enrichments (e.g., Lorand et al., 2021; Saunders et al., 2018). Comparably, mantle pyroxenites, which generally crystallize from mafic melts and commonly act as metasomatic agents in the upper mantle, show variably higher Pt, Pd, Au, Cu, and S, Re contents (e.g., Holwell et al., 2019; McInnes et al., 1999; Wang and Becker, 2015). Although mantle metasomatism by pyroxenite melts or volatile-rich melts may replenish sulfides and metals into the SCLM, these mediums only take up 5 - 10 % of shallow SCLM (Downes, 2007) and show contents of chalcophile metals that are similar to or slightly higher than the primitive mantle. (c) The enclosed sulfides in peridotites generally reflect the mantle residue upon partial melting, displaying high IPGE but lower PPGE, Au, Cu, and Re contents. In contrast, the interstitial sulfides with metasomatic origins display low IPGE (Os, Ir, Ru) but higher PPGE (Pt, Pd), Au, Cu, and S, Re contents, which are similar to those of pyroxenites-hosted sulfides. Notably, the absolute contents of chalcophile metals in metasomatic sulfides and pyroxenite-hosted sulfides are still lower than, or indistinguishable from enclosed sulfides (e.g., Alard et al., 2011; Saunders et al., 2016; Tassara et al., 2018). This explains why the metasomatic sulfides or metasomatized peridotites have high Os/Ir, Ru/Ir, and Pd/Ir ratios but their whole-rock chalcophile metal contents are still similar to or lower than the asthenospheric mantle. Consequently, mantle metasomatism related to subduction is difficult to result in large-scale enrichment of strongly chalcophile metals in the SCLM. Data sources: Fertile lherzolites, depleted harzburgites, and mantle pyroxenites (Fischer-Gödde et al., 2011; Wang and Becker, 2015), metasomatized peridotites (Alard et al., 2011; Holwell et al., 2019; Lorand et al., 2021; Maier et al., 2012; McInnes et al., 1999; Saunders et al., 2018; Wang et al., 2020b), enclosed sulfides and pyroxenites-hosted sulfides (Alard et al., 2011; Saunders et al., 2016), interstitial sulfides in metasomatized peridotites (Alard et al., 2011; Aulbach et al., 2021; Rielli et al., 2018; Tassara et al., 2018). Primitive mantle normalization values are from McDonough and Sun (1995) and Becker et al. (2006).